marine drugs

MDPI

Article

Anticancer Effect of Pacificusoside D from the Starfish *Solaster pacificus* in Combination with 2-Deoxy-D-glucose on Oxidative Phosphorylation in Triple-Negative Breast Cancer Cells MDA-MB-231

Olesya S. Malyarenko *, Timofey V. Malyarenko, Alla A. Kicha, Svetlana P. Ermakova and Natalia V. Ivanchina

G.B. Elyakov Pacific Institute of Bioorganic Chemistry, Far Eastern Branch of the Russian Academy of Sciences, 159 100-let Vladivostok Ave., Vladivostok 690022, Russia; malyarenko-tv@mail.ru (T.V.M.); kicha@piboc.dvo.ru (A.A.K.); swetlana_e@mail.ru (S.P.E.); ivanchina@piboc.dvo.ru (N.V.I.)
* Correspondence: malyarenko.os@gmail.com; Tel.: +7-(423)231-18-75; Fax: +7-(423)231-40-50

Abstract

Triple-negative breast cancer (TNBC) represents significant therapeutic challenges due to its aggressive behavior, metabolic plasticity, and lack of targeted treatments, prompting investigation of biologically active triterpene glycosides from the starfish *Solaster pacificus*. This study evaluated the ability of pacificusoside D (SpD) to synergistically enhance the anticancer efficacy of the glycolytic inhibitor 2-deoxy-D-glucose (2-DG) in TNBC MDA-MB-231 cells by targeting mitochondrial oxidative phosphorylation (OXPHOS). Methods included metabolic profiling via glucose uptake, lactate, and glutamate Glo assays; IC_{50} determination by MTS and trypan blue assays; colony formation evaluation using a soft agar assay; and molecular mechanism elucidation by Western blot, fluorescence microscopy and spectrometry, and flow cytometry analyses. Results demonstrated that MDA-MB-231 cells predominantly utilized glycolysis under basal conditions, shifting to OXPHOS with 2-DG (0.5 mM). IC_{50} values were 8.0/8.4 mM for 2-DG and 0.3/0.25 μM for SpD after 24 h of cell treatment. SpD exhibited a significant decrease in the number of colonies in MDA-MB-231 cells and possessed synergistic anticancer effects with 2-DG. Mechanistically, SpD increased tumor suppressor VHL expression level, down-regulated expression level of electron transport chain enzymes, generated reactive oxygen species, induced mitochondrial dysfunction, and triggered Bax/Bak-mediated apoptosis. These findings highlighted the synergistic anticancer potential of SpD in combination with 2-DG in aggressive breast cancer, offering insights into improved clinical outcomes in the future.

Keywords: triple-negative breast cancer; MDA-MB-231 cells; oxidative phosphorylation; 2-deoxy-D-glucose; *Solaster pacificus*; triterpene glycosides; pacificusoside D; anticancer effect; mitochondrial dysfunction; apoptosis induction

Check for updates

Academic Editors: Marc Diederich and Celso Alves

Received: 27 January 2026
Revised: 5 February 2026
Accepted: 10 February 2026
Published: 11 February 2026

Copyright: © 2026 by the authors. Licensee MDPI, Basel, Switzerland. This article is an open access article distributed under the terms and conditions of the Creative Commons Attribution (CC BY) license.

1. Introduction

Breast cancer remains the most frequently diagnosed malignancy among women globally, exerting profound impacts on health, quality of life, and survival [1]. In 2022, an estimated 2,296,840 new cases were reported worldwide, alongside 666,103 deaths, accounting for approximately 11% of all cancer incidences [2].

Breast cancer is classified into four main molecular subtypes: luminal A, luminal B, human epidermal growth factor receptor 2 (HER2)-positive, and triple-negative breast cancer (TNBC)—based on the presence or absence of estrogen receptor (ER), progesterone receptor (PR), and HER2 [3,4]. Among these, TNBC is particularly aggressive, accounts for roughly 20% of cases, and poses a significant threat to health, especially for younger women [5,6].

While clinical outcomes for breast cancer patients have improved over recent decades through advancements in therapies such as targeted agents, gene therapy, dendritic cell-based vaccines, monoclonal antibodies, chimeric antigen receptor (CAR) T-cell therapy, and oncolytic viruses, the median overall survival for TNBC remains limited to 10.2 months with these approaches [7–9]. This may partly be due to the fact that TNBC exhibits a hybrid metabolic phenotype characterized by metabolic plasticity, enabling dynamic shifts between aerobic glycolysis (the Warburg effect) and oxidative phosphorylation (OXPHOS). The metabolic plasticity of the TNBC cells provides adaptation to fluctuations in nutrients, hypoxia, and various stressors, thereby promoting rapid proliferation and invasion—hallmarks that significantly contribute to tumor aggressiveness and therapeutic resistance [10,11]. Thus, targeting cancer metabolism as a therapeutic strategy offers promise across various cancer types, including breast cancer.

Multiple pharmacological agents targeting glycolysis in tumors are currently being evaluated in preclinical models and clinical trials. 2-Deoxy-D-glucose (2-DG) represents the most extensively studied glucose metabolism-targeting agent in experimental and clinical oncology [12]. As a glucose analog, 2-DG competitively inhibits glucose transport through shared glucose transporters and is phosphorylated by hexokinase to form 2-deoxy-D-glucose-6-phosphate (2-DG6P), which cannot proceed through glycolysis or the pentose phosphate pathway, thereby suppressing ATP and NADPH production [13,14].

Beyond glycolytic inhibition, 2-DG induces endoplasmic reticulum (ER) stress through structural mimicry of mannose, disrupting oligosaccharide synthesis and N-linked glycosylation, which activates unfolded protein responses and ER stress pathways. Additionally, 2-DG modulates gene expression and protein phosphorylation involved in cell signaling, cycle regulation, DNA repair, calcium homeostasis, and apoptotic cell death [15–17].

The clinical application of 2-DG as monotherapy is limited by dose-dependent toxicity requiring chronic high-dose administration. Acute pharmacological doses of 2-DG produce hypoglycemia-like symptoms, primarily due to glucocytopenia in the hypothalamus, resulting in cardio-respiratory and immune system dysregulation [18].

Furthermore, administration of 2-DG at sublethal doses may induce metabolic reprogramming from glycolysis to OXPHOS in cancer cells, potentially promoting therapeutic resistance through the metabolic adaptability characteristic of aggressive tumor phenotypes [16,17]. Consequently, combinatorial therapeutic strategies employing bioactive compounds in combination with 2-DG represent a more promising approach to enhance treatment efficacy while simultaneously mitigating resistance mechanisms and reducing systemic toxicity [19,20].

The world's oceans have provided an abundance of natural resources exploited by mankind since time immemorial, historically used to sustain human life and as sources of biologically active substances. The value of these resources is well-established, with approximately 50% of existing pharmaceuticals derived from natural compounds [21,22]. Marine organisms, in particular, represent a unique source of diverse low-molecular-weight metabolites with substantial potential for therapeutic innovation [23]. For example, starfish, as active predators, synthesize a wide array of such metabolites, including peptides, sterols, polar steroids, glycosides, carotenoids, anthraquinone pigments, and sphingolipids [24]. Furthermore, their diet, which sometimes includes sea cucumbers or sea sponges, leads

them to accumulate secondary metabolites atypical to their own species, such as triterpene glycosides or alkaloids [25,26]. Oxidized steroid compounds from the starfish were considered to possess not only unique chemical structures but also diverse biological activities, including anticancer properties [27–31].

Recently, triterpene glycosides isolated from the Far Eastern starfish *Solaster pacificus*, namely cucumarioside D and pacificusosides D–K, demonstrated potent cytotoxic and colony-inhibiting effects on human melanoma cell lines SK-MEL-2, SK-MEL-28 and RPMI-7951. Pacificusosides F and H exhibited moderate cancer-preventive and anticancer effects in the models of neoplastic transformation of mouse epidermal cells JB6 Cl41 induced by carcinogens and in the colony formation of human melanoma cells SK-MEL-2, respectively. In contrast, pacificusoside I showed only slight activity in these assays. The difference in biological activity among these triterpene glycosides from the starfish *S. pacificus* appears to depend on the structure of both the triterpene aglycon (particularly its side chain) and the carbohydrate chain [29]. Moreover, pacificusoside D from the starfish *S. pacificus* was shown to possess synergistic radiomodifying activity with fucoidan from the brown alga *Saccharina cichorioides* in the models of cell viability and invasion of 3D SK-MEL-2 cells [30].

To the best of our knowledge, there are no prior reports in the literature on the anticancer effects of triterpene glycosides from the starfish in combination with the glycolytic inhibitor 2-DG on OXPHOS of cancer cells.

The present study aimed to evaluate the anticancer activity of cucumarioside D (CucD) and pacificusosides D (SpD), F (SpF), H (SpH), and I (SpI), isolated from the starfish *S. pacificus*, against TNBC MDA-MB-231 cells. In addition, the synergistic colony-inhibiting potential of SpD in combination with 2-DG in MDA-MB-231 cells and the underlying molecular mechanisms mediating its effects were also elucidated.

2. Results and Discussion

2.1. Structure of Triterpene Glycosides from the Starfish S. pacificus

In our recent study [29], we isolated triterpene glycosides, designated as pacificusosides D (SpD), F (SpF), H (SpH), and I (SpI), along with the previously known cucumarioside D (CucD), from the starfish *S. pacificus*. These compounds were purified by column chromatography using Polychrome 1 and silica gel, followed by semi-preparative HPLC on Diasorb-130-C16T, Diasfer-110-C18, and Discovery C18 columns. The structures of the isolated compounds were determined by ^{1}H, ^{13}C NMR, and ESI MS spectra.

The triterpene glycosides CucD and SpD are characterized by a holostane-type aglycon featuring a 16β-OAc group and a 7(8)-double bond in the nucleus, along with *cis*- or *trans*-$\Delta^{22,24}$ side chains, respectively. Both compounds share an identical carbohydrate chain composed of five monosaccharide units: two β-D-xylopyranosyl, β-D-quinovopyranosyl, β-D-glucopyranosyl, and 3-*O*-methyl-β-D-glucopyranosyl attached to the C-3 position of the aglycon (Figure 1). Compounds SpH and SpF have holostane-type aglycons similar to those of CucD and SpD, respectively, but differ in their carbohydrate moieties. Specifically, SpH and SpF contain a tetrasaccharide chain consisting of β-D-xylopyranosyl, β-D-quinovopyranosyl, 6-*O*-sulfo-β-D-glucopyranosyl, and 3-*O*-methyl-β-D-xylopyranosyl residues. Finally, SpI is distinguished by a unique 23,24,25,26,27-penta*nor*-lanosta-7,20(22)-diene-18(16)-lactone-3β-ol aglycon and a pentasaccharide carbohydrate chain identical to that of CucD and SpD (Figure 1).

It is known that the main secondary metabolites of starfishes (Asteroidea, Echinodermata) are polyhydroxysteroids and their glycosides. In contrast, triterpene glycosides are characteristic compounds of sea cucumbers (Holothuroidea, Echinodermata). We previously proposed that certain predatory starfish species, which feed on sea cucumbers, not only accumulate these triterpene glycosides but also partially modify them [29,31,32]. Given

the structural similarities between the triterpene glycosides isolated from the starfish *S. pacificus* and those from sea cucumbers of the genus Eupentacta, it can be hypothesized that the starfish *S. pacificus* primarily feeds on these sea cucumbers. Consequently, triterpene glycosides may serve as reliable food chain markers in this predator-prey relationship.

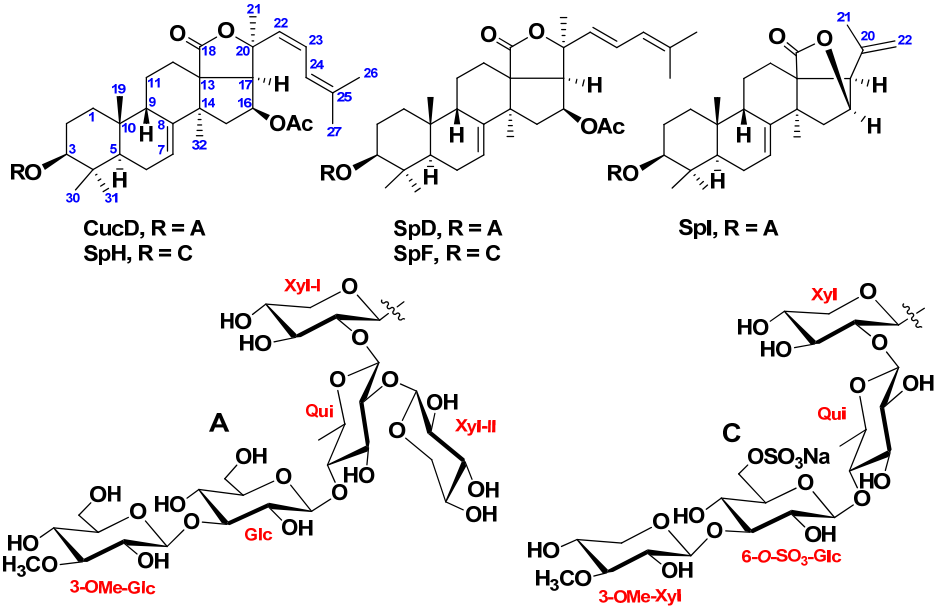


Figure 1. Structures of triterpene glycosides CucD, SpD, SpF, SpH, and SpI from the starfish *S. pacificus*. Xyl: β-D-xylopuranose, Qui: β-D-quinovopuranose, Glc: β-D-glucopuranose, 3-OMe-Glc: 3-O-methyl-β-D-glucopuranose, 3-OMe-Xyl: 3-O-methyl-β-D-xylopuranose, 6-O-SO_3-Glc: 6-O-sulfoxy-β-D-glucopuranose.

2.2. The Effect of 2-DG on the Metabolic Profile, Viability and Proliferation of Human TNBC Cells MDA-MB-231

One of the key factors underlying the aggressiveness of TNBC cells is their metabolic plasticity, which enables adaptive reprogramming to sustain proliferation, invasion, and survival under stress [33]. In this study, the metabolic profile of TNBC cells MDA-MB-231 and the effect of 2-DG on their metabolic plasticity were assessed through the glucose uptake and the excretion/production of lactate and glutamate, key indicators of glycolytic and OXPHOS activity, respectively.

Untreated MDA-MB-231 cells exhibited robust glucose uptake, consuming 91 μM of glucose (Figure 2a). Lactate, a product of glycolysis, was predominantly excreted into the culture medium, reaching 36 μM, while glutamate, associated with OXPHOS and amino acid metabolism, accumulated intracellularly at 28 μM (Figure 2a). These findings and recent literature data [34,35] support that MDA-MB-231 cells efficiently utilize glucose and support both glycolytic and OXPHOS metabolic pathways, with glycolysis appearing predominant under basal conditions (Figure 2a).

Targeted disruption of cancer cell metabolism represents a promising strategy for anticancer therapy [36,37]. 2-DG, a glucose analog that inhibits glycolysis by competitively binding hexokinase, is commonly employed as a metabolic modulator to impair glycolysis and consequently suppress cancer cell proliferation [14,38]. However, certain cancers can reprogram their metabolism in response to inhibitors, potentially limiting therapeutic efficacy and fostering resistant subpopulations [11,39].

We checked the idea that the treatment of glycolytically active MDA-MB-231 cells by 2-DG might induce a metabolic shift toward mitochondrial OXPHOS, sustaining cell proliferation and cancer development.

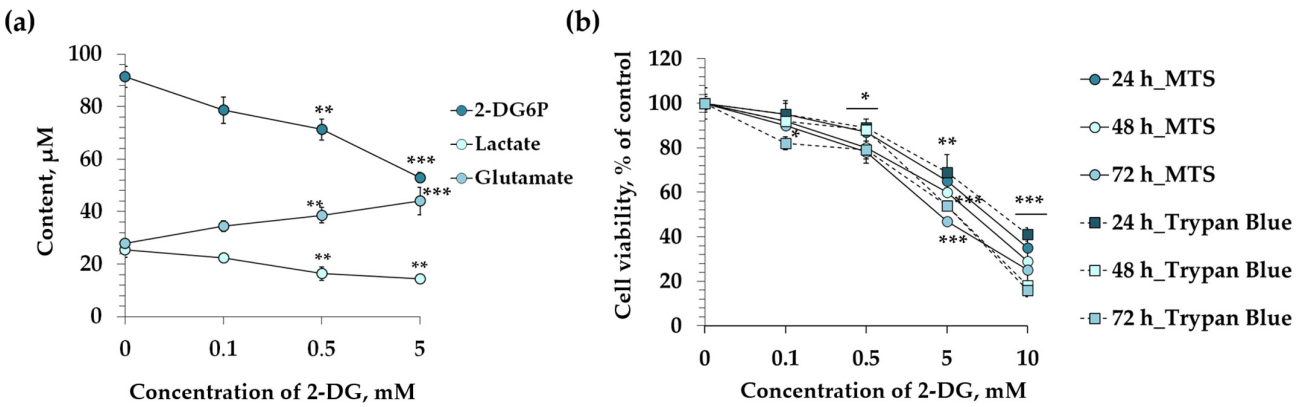


Figure 2. The effect of 2-DG on the metabolic profile, cell viability, and proliferation of TNBC cells MDA-MB-231. (**a**) MDA-MB-231 cells (5×10^3 cells/200 µL) were treated with either DMSO (vehicle control) or 2-DG at 0.1, 0.5, 5 mM and incubated for 24 h. The ability of MDA-MB-231 cells to take up glucose, excrete the lactate and glutamate, as determined by Glucose uptake or Lactate/Glutamate Glo assays. (**b**) MDA-MB-231 cells (1×10^4 cells/200 µL) were treated with either DMSO (vehicle control) or 2-DG at 0.1, 0.5, 5, and 10 mM and incubated for a time point of 24, 48, or 72 h as compared to DMSO-treated cells (control). Cell viability was estimated by the MTS and trypan blue exclusion assays. Data show the mean of three independent experiments ± SD. The asterisks indicate (**a**) a significant changes in the content of 2-deoxy-D-glucose-6-phosphate (2-DG6P), lactate and glutamate or (**b**) a significant decrease in cell viability of MDA-MB-231 cells treated with different concentrations of 2-DG at one time point of 24 or 48 or 72 h as compared to DMSO-treated cells (control) (* $p < 0.05$; ** $p < 0.01$; *** $p < 0.001$).

Consistent with its mechanism, 2-DG dose-dependently suppressed glucose uptake by 14%, 22%, and 42% at concentrations of 0.1, 0.5, and 5 mM, respectively, and reduced lactate excretion by 19%, 27%, and 50%, respectively, compared to DMSO-treated cells (control) (Figure 2a). Conversely, 2-DG significantly elevated intracellular glutamate levels by 23%, 38%, and 57% at the same concentrations, indicative of a compensatory upregulation in OXPHOS-dependent metabolism (Figure 2a).

The effects of 2-DG on the proliferation of TNBC cells MDA-MB-231 were evaluated (Figure 2b). The half-maximal inhibitory concentration (IC_{50}) of 2-DG in MDA-MB-231 cells after 24 h of treatment was determined to be 8.0 ± 0.5 mM (MTS assay) and 8.4 ± 0.7 mM (Trypan blue exclusion assay), demonstrating consistent cytotoxicity across both methods. This concordance confirms that the cytotoxic effect of 2-DG is not mediated through direct inhibition of mitochondrial succinate dehydrogenase (SDH), as the MTS assay—reliant on SDH-mediated reduction of tetrazolium salts—remains unaffected at biologically relevant concentrations. Thus, the observed cell death is attributable to glycolytic inhibition rather than off-target disruption of mitochondrial electron transport chain function. 2-DG (0.1, 0.5, 5, and 10 mM) inhibited growth of MDA-MB-231 cells in a dose- and time-dependent manner by 5%, 13%, 35%, and 65% after 24 h of cell treatment;—by 8%, 20%, 40%, and 71% after 48 h of cell treatment; and—by 10%, 22%, 52%, and 75% after 72 h of cell treatment, compared to DMSO-treated cells (control) (Figure 2b).

Results obtained demonstrated that TNBC cells MDA-MB-231 exhibit metabolic adaptation under 2-DG treatment at lower doses (e.g., 0.5 mM), reprogramming their metabolism by shifting from glycolysis toward OXPHOS. The 2-DG at a low concentration of 0.5 mM slightly inhibited cell viability and proliferation of MDA-MB-231 cells even in 72 h of cell treatment, highlighting a significant risk of therapeutic resistance in TNBC and complicating therapeutic efforts. That is why the search and development of novel compounds capable of effectively suppressing the development and progression of aggressive cancers

targeting multiple facets of cancer cell metabolism is an urgent task to circumvent resistance mechanisms and improve clinical outcomes in TNBC.

2.3. The Effect of Triterpene Glycosides from the Starfish S. pacificus on the Viability of Human TNBC Cells MDA-MB-231

In this study, we evaluated the effect of triterpene glycosides CucD, SpD, SpF, SpH, and SpI from the starfish *S. pacificus* on the viability of TNBC cells MDA-MB-231 in order to calculate their half-maximal inhibitory concentration (IC_{50}) and selectivity index (SI), and identify effective concentrations for subsequent experiments.

The IC_{50} of CucD, SpD, SpF, SpH, and SpI for MDA-MB-231 cells was 0.4/0.7, 0.3/0.25, 1.4/1.2, 1.3/1.4, and 1.6/1.79 μM, respectively, after 24 h of cell treatment as determined by MTS and Trypan blue exclusion methods (Table 1). Notably, all investigated compounds demonstrated a high SI and exerted cytotoxic effect on the viability of normal human embryonic kidney cells (HEK 293) with higher IC_{50} values compared to MDA-MB-231 cells following 24 h of treatment (Table 1).

Table 1. Cytotoxicity and selectivity index of triterpene glycosides from the starfish *S. pacificus*.

Compound	IC_{50} *, μM		SI *
	HEK293	MDA-MB-231	
	MTS/Trypan Blue		
CucD	3.8 ± 0.2/4.4 ± 0.5	0.4 ± 0.06/0.7 ± 0.02	9.5/6.3
SpD	2.5 ± 0.08/1.9 ± 0.2	0.3 ± 0.01/0.25 ± 0.04	8.3/7.6
SpF	5.9 ± 0.09/5.5 ± 0.05	1.4 ± 0.08/1.2 ± 0.1	4.2/4.6
SpH	5.8 ± 0.08/6.0 ± 0.1	1.3 ± 0.1/1.4 ± 0.05	4.4/4.3
SpI	4.6 ± 0.04/4.3 ± 0.06	1.6 ± 0.09/1.79 ± 0.03	2.9/2.4

***IC_{50}**—the concentration of compounds that caused a 50% reduction in cell viability of tested normal and cancer cells. Values are expressed as mean ± standard deviation. **SI**—the selectivity index, calculated as SI = (mean IC_{50} for normal cells)/(mean IC_{50} for cancer cells). Higher SI values indicate greater selectivity toward cancer cells.

Recently, the cytotoxic activity of triterpene glycosides, pacificusoside A–C, cucumariosides C_1, C_2, and A_{10} from the starfish *S. pacificus* was determined on the model of viability of human breast cancer cells MDA-MB-231, and colorectal carcinoma cells HT-29 [31], as well as the cytotoxicity of SpD, SpF, SpH, SpI, and CucD, was investigated against melanoma cells SK-MEL-2, SK-MEL-28, and RPMI-7951 [29]. IC_{50} values for triterpene glycosides from the starfish *S. pacificus* were shown to vary by compound and cell line, but are generally in the low-micromolar to sub-micromolar range for the most active saponins.

The working concentrations for 2-DG and the triterpene glycosides CucD, SpD, SpF, SpH, and SpI from the starfish *S. pacificus* were rationally selected based on preliminary data from cell proliferation and viability assays, respectively. For 2-DG, a concentration range of 0.1, 0.5, and 2.5 mM was chosen. These concentrations were selected because they have been shown to effectively induce a metabolic shift from glycolysis to OXPHOS in MDA-MB-231 cells without significant effects on cell proliferation, thereby allowing us to focus on its metabolic impact.

A common set of concentrations (0.05, 0.1, and 0.2 μM) was selected to assess the colony-inhibiting effects of all investigated triterpene glycosides to facilitate a direct comparative analysis of their bioactivities. The highest concentration in this range (0.2 μM) was defined as half the IC_{50} value of the most cytotoxic triterpene glycosides CucD and SpD.

2.4. The Effect of 2-DG and Triterpene Glycosides from the Starfish S. pacificus on the Colony Formation in Human TNBC Cells MDA-MB-231

The effect of 2-DG and the investigated triterpene glycosides SpD, SpF, SpH, SpI, and CucD from the starfish *S. pacificus* at non-toxic concentrations on the colony formation in TNBC cells MDA-MB-231 was estimated using the soft agar clonogenic assay.

Soft agar clonogenic assay is a cornerstone of in vitro cancer research, evaluating the clonogenic potential of cancer cells—their ability to proliferate and form colonies under anchorage-dependent conditions [40]. This assay mimics tumor initiation and metastatic spread, providing insights into cellular proliferation, survival, and resistance mechanisms [41]. In TNBC, which is characterized by aggressive growth, chemoresistance, and poor prognosis, colony formation assays are particularly valuable for assessing therapeutic efficacy and identifying novel compounds that inhibit cancer cell expansion.

Initially, the effect of 2-DG, CucD, SpD, SpF, SpH, and SpI was assessed individually. The treatment with 2-DG at concentrations of 0.1, 0.5, and 2.5 mM reduced the number of colonies in MDA-MB-231 cells by 17%, 29%, and 86%, respectively, compared to the DMSO-treated cells (control) (Figure 3a). Among the triterpene glycosides, CucD and SpD exhibited the highest colony-inhibiting efficacy. CucD at 0.05, 0.1, and 0.2 μM inhibited colony formation in MDA-MB-231 cells by 11%, 24%, and 67%, respectively (Figure 3b), while SpD at the same concentrations suppressed colony growth by 37%, 56%, and 86%, respectively, compared to control (Figure 3c). In contrast, SpF, SpH, and SpI were less effective than CucD and SpD, with the inhibition percentages below 30% at 0.2 μM (Figure 3d–f).

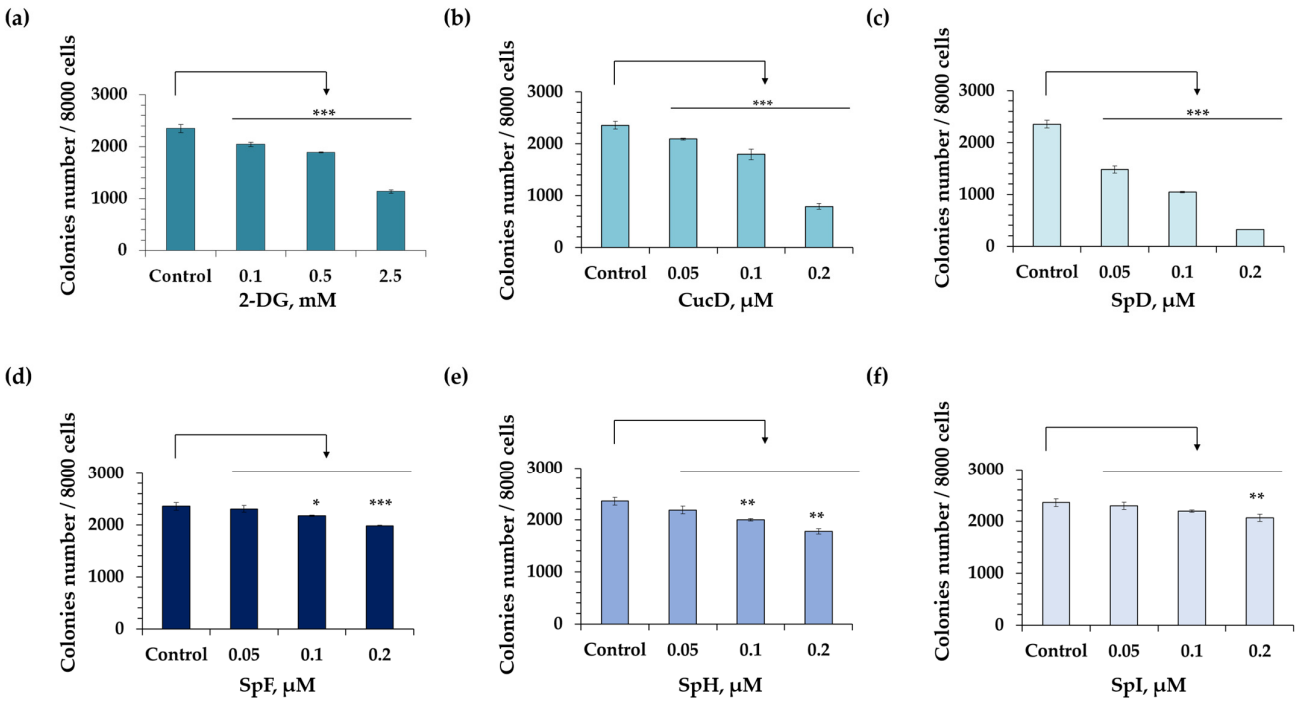


Figure 3. The effect of 2-DG, CucD, SpD, SpF, SpH, and SpI from the starfish *S. pacificus* on the colony formation in TNBC cells MDA-MB-231. MDA-MB-231 cells were treated with (**a**) 2-DG at concentrations of 0.1, 0.5, and 2.5 mM; (**b**) CucD; (**c**) SpD; (**d**) SpF; (**e**) SpH; (**f**) SpI at concentrations of 0.05, 0.1, and 0.2 μM in soft agar. The number of colonies was counted under a Motic AE 20 microscope (total magnification of 10×) using ImageJ version 1.50i software bundled with 64-bit Java 1.6.0_24. Results are presented as mean ± standard deviation (SD). The asterisks indicate a significant decrease in the number of colonies in MDA-MB-231 cells treated with different concentrations of 2-DG and triterpene glycosides from the starfish *S. pacificus* as compared to DMSO-treated cells (control) (* $p < 0.05$; ** $p < 0.01$; *** $p < 0.001$).

Since SpD from the starfish *S. pacificus* possessed potent cytotoxic and colony-inhibiting activity against TNBC cells MDA-MB-231, it was chosen for the investigation of its metabolic effects and molecular mechanism of action.

For this reason, MDA-MB-231 cells were pre-treated with 2-DG (0.5 mM), followed by exposure to SpD at non-toxic concentrations of 0.025, 0.05, and 0.1 μM. The results demonstrated that 2-DG alone slightly reduced colony formation by 14%, compared to DMSO-treated cells (control) (Figure 4a,b). SpD at 0.025, 0.05, and 0.1 μM was shown to inhibit the colony growth by 10%, 32%, and 52%, respectively, compared to the control. Notably, SpD (0.025, 0.05, and 0.1 μM) in combination with 2-DG (0.5 mM) decreased colony number in MDA-MB-231 cells by 61%, 72%, and 81%, respectively, compared to cells treated with 2-DG only (Figure 4a,b). These findings demonstrated the synergistic potential of combining metabolic modulator such as 2-DG with triterpene glycosides to enhance therapeutic efficacy against TNBC.

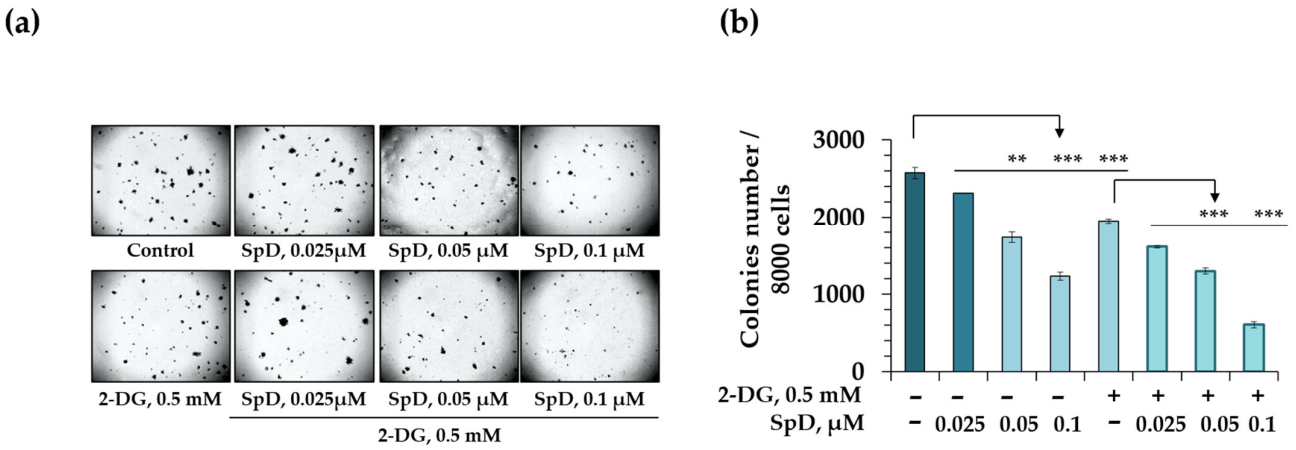


Figure 4. The effect of SpD from the starfish *S. pacificus* in combination with 2-DG on the colony formation in TNBC cells MDA-MB-231. (**a**,**b**) MDA-MB-231 cells were pre-treated with 2-DG at concentrations of 0.5 mM and then treated with SpD at concentrations of 0.025, 0.05, and 0.1 μM in soft agar. The number of colonies was counted under a Motic AE 20 microscope (total magnification of 10×) using ImageJ version 1.50i software bundled with 64-bit Java 1.6.0_24. Results are presented as mean ± standard deviation (SD). The one-way ANOVA and the Tukey's HSD test for multiple comparisons show statistical significance as compared to DMSO-treated cells (control) or 2-DG-treated cells (** $p < 0.01$; *** $p < 0.001$).

In the present study, we tested the hypothesis that treatment of TNBC cells MDA-MB-231 with 2-DG at a low dose of 0.5 mM would shift cellular metabolism from glycolysis toward OXPHOS, and that subsequent treatment by SpD from the starfish *S. pacificus* would result in pronounced inhibition of colony formation in MDA-MB-231 cells via modulation of OXPHOS.

2.5. The Molecular Mechanism of the Effect of SpD from the Starfish S. pacificus in Combination with 2-DG in Human TNBC Cells MDA-MB-231

TNBC cells frequently exhibit a metabolic preference for glycolysis (the Warburg effect), characterized by elevated glucose uptake and lactate production even under aerobic conditions, which supports rapid proliferation and evasion of oxidative stress [42,43]. Therapeutic interventions, such as the use of the inhibitor of glycolysis, such as 2-DG, can induce metabolic reprogramming toward OXPHOS, shifting cellular reliance from glycolytic ATP production to mitochondrial respiration [18,44]. This reprogramming is mediated by tumor suppressor von Hippel-Lindau (VHL), which destabilizes hypoxia-inducible factor 1α (HIF-1α) and promotes mitochondrial biogenesis and electron transport

chain (ETC) activity [45]. Specifically, VHL-driven reprogramming activates key mitochondrial ETC components, including ubiquinol-cytochrome c reductase core protein 2 (UQCRC2) in complex III, cytochrome c oxidase subunit 1 (COX1) in complex IV, and ATP synthase subunit alpha (ATP5a1) in complex V [46]. It was reported that overexpression of mitochondrial ETC components was observed in various cancers and associated with poor prognosis in hepatocellular [47], gastric [48], colorectal [49] and ovarian [50] cancers. These findings emphasize the therapeutic potential of modulation of the expression level of ETC components in TNBC to target cancer cell metabolism and disrupt tumor progression.

Therefore, we determined the effect of SpD from the starfish *S. pacificus* on 2-DG-inducing OXPHOS, ultimately regulating the expression level of tumor suppressor VHL, and the components of mitochondrial electron transport chain (ETC), as well as the reactive oxygen species (ROS) production, and the induction of apoptosis in TNBC cells MDA-MB-231.

At first, the effect of SpD on the alteration of the expression level of VHL, UQCRC2, COX1, and ATP5a1 in TNBC cells MDA-MB-231 under 2-DG treatment was quantified using Western Blot assay (Figure 5a,b).

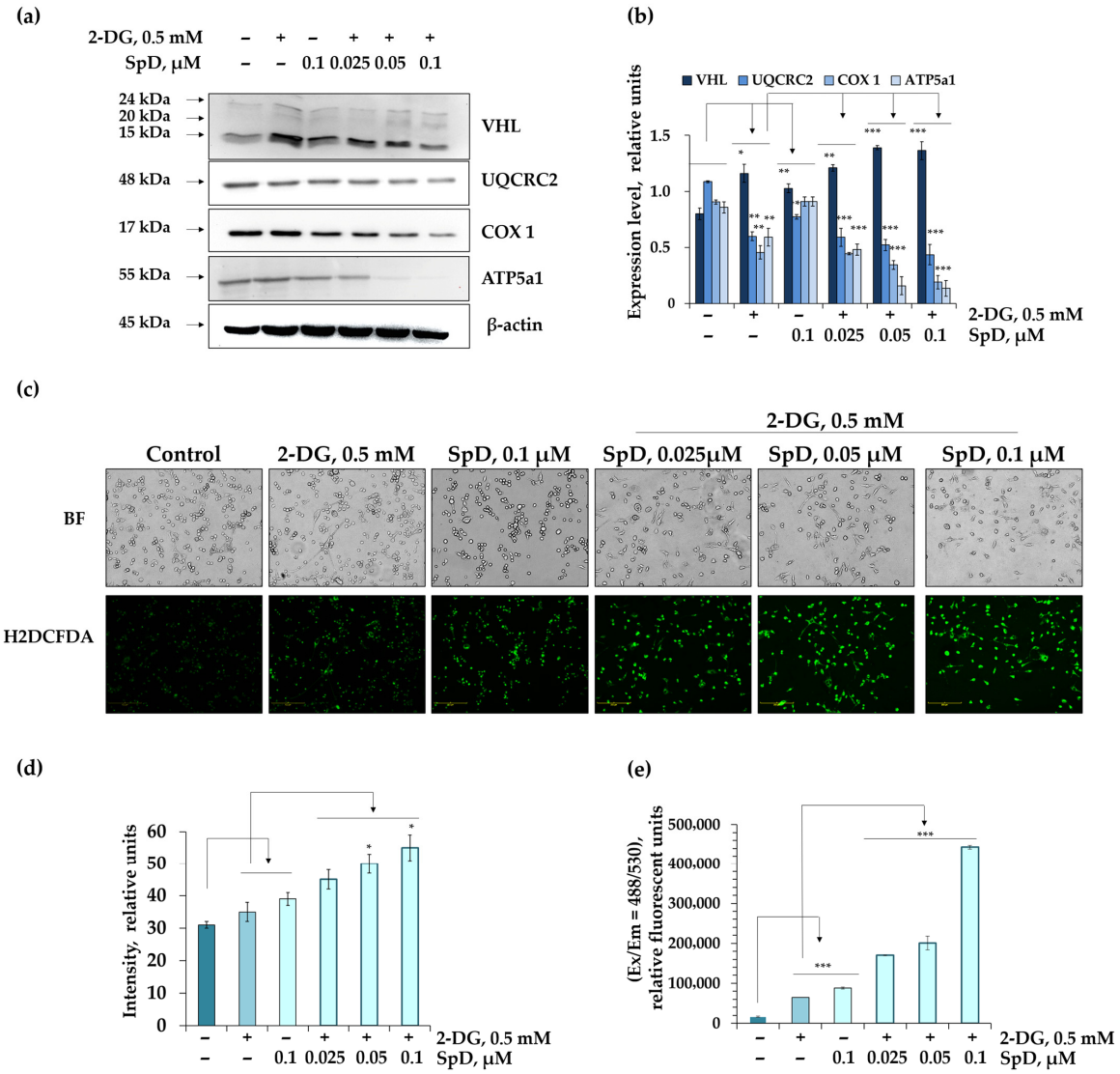


Figure 5. The effect of SpD from the starfish *S. pacificus* in combination with 2-DG on the expression level of enzymes of mitochondrial complexes and ROS generation in TNBC cells MDA-MB-231. MDA-MB-231

cells were treated by either 2-DG (0.5 mM) or SpD (0.1 μM) alone or by 2-DG (0.5 mM) in combination with SpD (0.025, 0.05, and 0.1 μM) and subjected to Western Blot or fluorescence microscopy and spectrometry assays. (**a**) The regulation of the expression level of VHL tumor suppressor, UQCRC2 (complex III), COX1 (complex IV), ATP5a1 (complex V), and β-actin was quantified by Western Blot assay. (**b**) Relative expression level was measured using the Quantity One 1D analysis version 4.6.7 software. Expression level was normalized to the total level of β-actin. (**c**) Fluorescence microscopic images were taken under CELENA® X High Content Imaging System at a total magnification of 10×, aided with cell-integrated CELENA® X Cell Analyzer software version 1.6.0. (**d**) Fluorescence intensity of H_2DCFDA in MDA-MB-231 cells was determined by ImageJ version 1.50i software bundled with 64-bit Java 1.6.0_24. (**e**) Fluorometric quantification of ROS level by Synergy H1 multimode microplate reader. Results are expressed as mean ± SD. The one-way ANOVA and the Tukey's HSD test for multiple comparisons show statistical significance as compared to DMSO-treated cells (control) or 2-DG-treated cells (* $p < 0.05$; ** $p < 0.01$; *** $p < 0.001$).

The treatment of MDA-MB-231 cells with 2-DG (0.5 mM) alone upregulated the expression level of VHL tumor suppressor, leading to upregulation of ETC enzymes expression, namely UQCRC2, COX1, and ATP5a1. This confirmed enhancement of mitochondrial respiratory chain activity during the metabolic shift from glycolysis to OXPHOS. SpD at concentrations of 0.025, 0.05, and 0.1 μM in combination with 2-DG (0.5 mM) up-regulated the expression level of VHL by 6%, 29%, and 25%, respectively, compared to cells treated by 2-DG only (Figure 5a,b). However, SpD (0.025, 0.05, and 0.1 μM) reduced the expression of UQCRC2 by 1%, 6%, and 8%, respectively; COX1—by 1%, 12%, and 29%, respectively; and ATP5a1—by 13%, 50%, and 53%, respectively, compared to 2-DG treated cells (Figure 5a,b). It should be noted that SpD exhibited the strongest inhibitory effect on ATP5a1, targeting the late stages of OXPHOS. These results indicated that SpD down-regulated ETC complex efficiency, impairing mitochondrial function and modulated 2-DG-induced OXPHOS in TNBC cells MDA-MB-231.

Mitochondria are primary sources of ROS, which are byproducts of OXPHOS, mediating signaling and oxidative stress [51]. During the glycolysis-to-OXPHOS shift, ETC activation (complexes III, IV, V) leads to the production of ROS, which can overload antioxidant defenses and induce mitochondrial dysfunction. Next, we checked whether SpD impaired ETC efficiency, causing electron leakage, which would increase ROS levels, thereby promoting mitochondrial dysfunction in MDA-MB-231 cells. Accordingly, the effect of SpD on 2-DG-induced generation of ROS was assessed by staining MDA-MB-231 cells with the cell-permeable fluorescent dye 2′,7′-dichlorodihydrofluorescein diacetate (H_2DCFDA), which is extremely sensitive to changes in redox state of the cells and capable of tracking ROS levels over time [52]. It was shown that 2-DG at a dose of 0.5 mM induced intracellular ROS generation by 13% compared to DMSO-treated cells (control), while 2-DG (0.5 mM) in combination with SpD at concentrations of 0.025, 0.05, and 0.1 μM significantly increased ROS levels by 16%, 30%, and 44%, respectively, compared to 2-DG-treated MDA-MB-231 cells. This elevation exacerbates electron ETC stress, contributing to oxidative damage in MDA-MB-231 cells. Consequently, SpD demonstrates substantial potential as an inducer of ROS-mediated oxidative stress, which could enhance therapeutic strategies targeting cancer cell death through metabolic disruption (Figure 5c–e).

Changes in mitochondrial mass serve as a critical biomarker of both physiological and pathological processes, reflecting overall cellular health and responding to factors such as oxidative stress and apoptosis [53]. For instance, oxidative stress can impair mitochondrial function, leading to dysfunction and induction of apoptosis [54]. In this study, we measured changes in mitochondrial mass in MDA-MB-231 cells under 2-DG-induced metabolic reprogramming combined with SpD treatment. The treatment of MDA-MB-231 cells with 2-DG (0.5 mM) in combination with SpD (0.025, 0.05, and 0.1 μM) resulted in decreases of mitochondrial mass by 4%, 5%, and 8%, respectively, compared to 2-DG-treated cells

(Figure 6a,b). Flow cytometric analysis of MitoTracker Green staining confirmed a dose-dependent reduction in mitochondrial mass in MDA-MB-231 cells treated with 2-DG (0.5 mM) in combination with SpD (0.025, 0.05, and 0.1 µM), resulting in decreases of 14%, 19%, and 35%, respectively, compared to cells treated with 2-DG alone (Figure 6c,d).

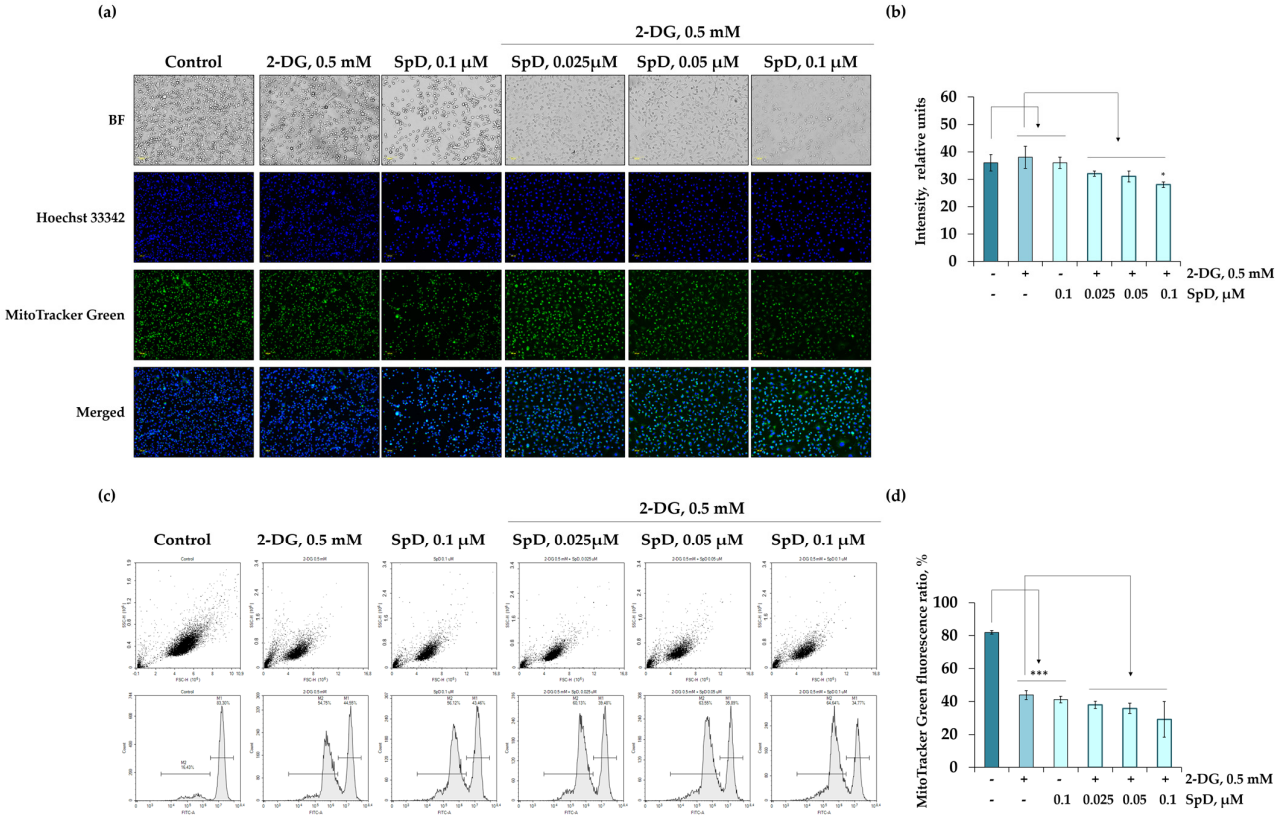


Figure 6. The effect of SpD from the starfish *S. pacificus* in combination with 2-DG on the alteration of mitochondrial mass in TNBC cells MDA-MB-231. MDA-MB-231 cells were treated with either 2-DG (0.5 mM) or SpD (0.1 µM) alone or by 2-DG (0.5 mM) in combination with SpD (0.025, 0.05, and 0.1 µM) and subjected to fluorescence microscopy and flow cytometry assays. (**a**) Fluorescence microscopic images were taken under CELENA® X High Content Imaging System (at a total magnification of 10×), aided with cell-integrated CELENA® X Cell Analyzer software version 1.6.0. (**b**) Fluorescence intensity of MitoTracker Green in MDA-MB-231 cells was determined by ImageJ version 1.50i software bundled with 64-bit Java 1.6.0_24. (**c**) Flow cytometry analysis of MDA-MB-231 cells stained with MitoTracker Green dye. (**d**) Quantitative calculation of the data obtained by NovoExpress flow cytometry software (version 1.6.1). Results are expressed as mean ± SD. The one-way ANOVA and the Tukey's HSD test for multiple comparisons show statistical significance as compared to DMSO-treated cells (control) or 2-DG-treated cells (* $p < 0.05$; *** $p < 0.001$).

The data obtained underscore the capability of SpD to elevate mitochondrial dysfunction in MDA-MB-231 cells induced by ROS-mediated oxidative stress, offering insights into targeting the metabolic plasticity of aggressive breast cancer cells.

The accumulated ROS, ETC stress, and mitochondrial dysfunction are known to induce apoptosis by the activation of pro-apoptotic proteins Bax (Bcl-2-associated X protein) and Bak (Bcl-2 antagonist/killer), which are pore-forming proteins that oligomerize on the mitochondrial outer membrane and induce mitochondrial outer membrane permeabilization (MOMP) [55–57]. MOMP releases cytochrome C, which assembles with apoptotic protease-activating factor 1 (Apaf-1) to form the apoptosome, activating initiator caspase 9. In turn, caspase 9 activates downstream effector caspase 7 and caspase 3, committing cells to apoptosis via proteolytic cascades [58–60].

It was shown that 2-DG (0.5 mM) and SpD (0.1 µM) alone slightly up-regulated the expression level of pro-apoptotic proteins Bax and Bak (Figure 7a,b). However, SpD at concentrations of 0.025, 0.05, and 0.1 µM in combination with 2-DG (0.5 mM) significantly up-regulated Bax expression by 31%, 42%, and 57%, respectively, and Bak expression by 5%, 21%, and 43%, respectively, compared to cells treated with 2-DG alone (Figure 7a,b). Moreover, the combination treatment with SpD (0.025, 0.05, and 0.1 µM) and 2-DG (0.5 mM) down-regulated caspase 9 activity by 19%, 28%, and 47%, respectively; caspase 7—by 8%, 20%, and 28%, respectively; and caspase 3—by 2%, 9%, and 16%, respectively, compared to 2-DG-treated cells. Finally, the combinatorial treatment of MDA-MB-231 cells with 2-DG and SpD induced cleavage of caspase 3, confirming induction of apoptosis in MDA-MB-231 cells (Figure 7a,b).

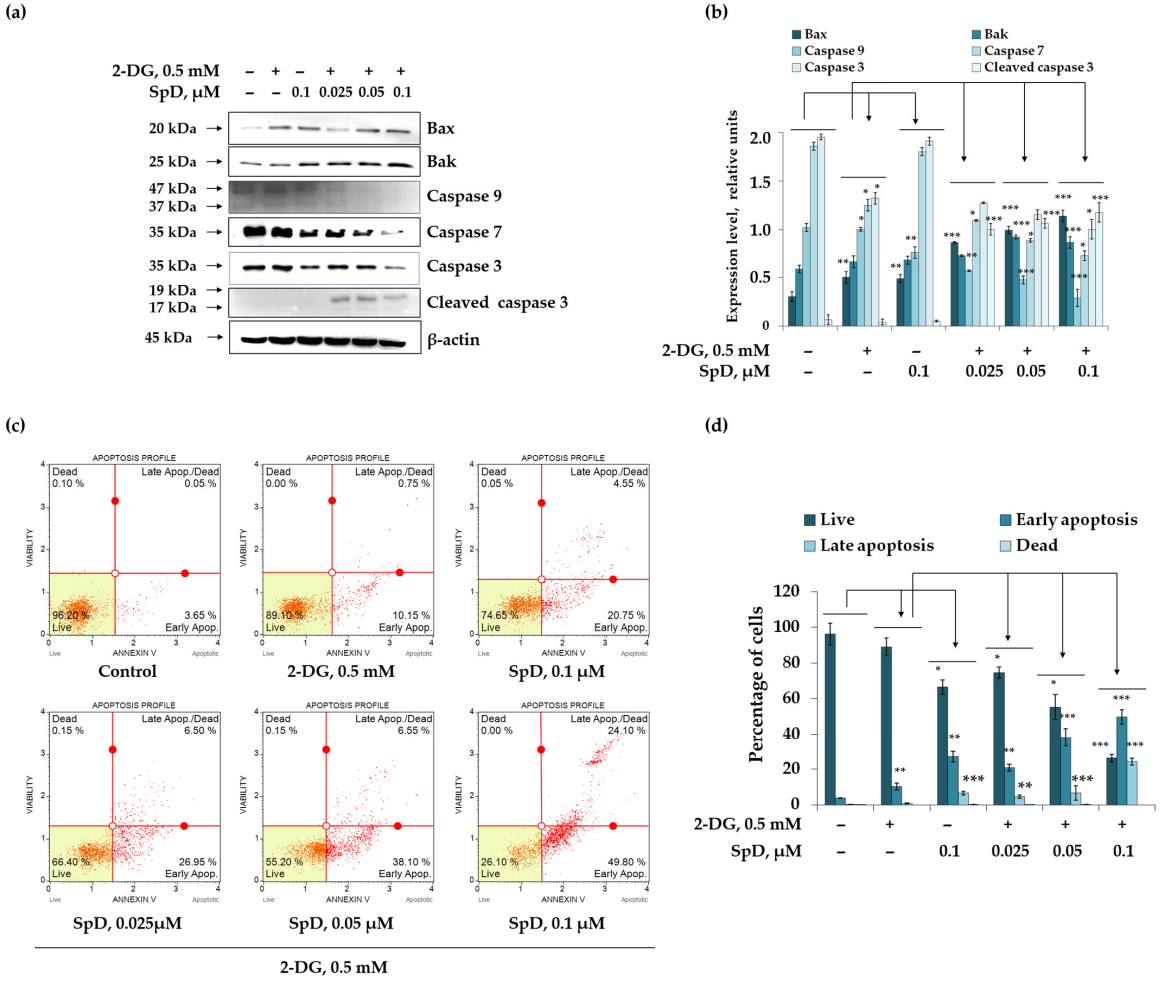


Figure 7. The effect of SpD from the starfish *S. pacificus* in combination with 2-DG on apoptosis induction in TNBC cells MDA-MB-231. (**a**) MDA-MB-231 cells were treated by either 2-DG (0.5 mM) or SpD (0.1 µM) alone or by 2-DG (0.5 mM) in combination with SpD (0.025, 0.05, and 0.1 µM). The regulation of the expression level of Bax, Bak, caspase 9, caspase 7, caspase 3, cleaved caspase 3, and β-actin were quantified by Western Blot assay. (**b**) Relative expression level was measured using the Quantity One 1D analysis version 4.6.7 software. Expression level was normalized to the total level of β-actin. (**c**) Dot plots show a representative experiment of treatments. (**d**) Bar charts show percentage values of live, early apoptotic, late apoptotic/dead, and dead MDA-MB-231 cells treated by 2-DG (0.5 mM) or SpD (0.1 µM) alone or by 2-DG (0.5 mM) in combination with SpD (0.025, 0.05, and 0.1 µM). Results are presented as mean ± standard deviation (SD). The one-way ANOVA and the Tukey's HSD test for multiple comparisons show statistical significance as compared to DMSO-treated cells (control) or 2-DG-treated cells (* $p < 0.05$; ** $p < 0.01$; *** $p < 0.001$).

Furthermore, we validated the apoptosis-inducing potential of SpD from the starfish *S. pacificus* in 2-DG-treated MDA-MB-231 cells using the Muse® Annexin V and Dead Cell Kit. As illustrated in Figure 7c,d, 2-DG (0.5 mM) or SpD (0.1 μM) alone slightly induced apoptosis, resulting in a modest increase in the percentage of early and late apoptotic cells. However, combinatorial treatment of TNBC cells MDA-MB-231 with 2-DG (0.5 mM) and SpD (0.025, 0.05, and 0.1 μM) markedly elevated the percentages of early apoptotic cells by 11%, 28%, and 40%, respectively, and late/dead apoptotic cells—by 4%, 6%, and 23%, respectively, compared to cells treated with 2-DG alone (Figure 7c,d).

Overall, these results highlight synergistic enhancement of apoptotic pathways by SpD from the starfish *S. pacificus* with inhibitor of glycolysis, 2-DG, in TNBC cells MDA-MB-231, supporting its potential as a promising therapeutic agent against aggressive breast cancer through OXPHOS-mediated molecular mechanisms (Figure 7).

3. Materials and Methods

3.1. Reagents

The phosphate-buffered saline (PBS), L-glutamine, penicillin/streptomycin solution (10,000 U/mL, 10 μg/mL), Dulbecco's Modified Eagle's Medium, Oligomycin, and 2-Deoxy-D-glucose were purchased from Sigma-Aldrich (St. Louis, MO, USA).

The MTS reagent 3-[4,5-dimethylthiazol-2-yl]-2,5-diphenyltetrazolium bromide, Glucose uptake Glo™ Assay kit, Lactate Glo™ Assay kit, and Glutamate Glo™ Assay kit were purchased from Promega (Madison, WI, USA). Trypan blue stain was purchased from Servicebio (Wuhan, Hubei, China). The trypsin, fetal bovine serum (FBS), and the protein marker PageRulerTM Plus Prestained Protein Ladder were purchased from Thermo Fisher Scientific (Waltham, MA, USA).

The cell lysis buffer (10×), Apoptosis Antibody Sampler Kit #9915, Pro-Apoptosis Bcl-2 Family Antibody Sampler Kit #9942, COX1 #4841, ATP5B (E8A5A) #85001, UQCRC2 (F8Y5N) #99258, VHL #68547 antibodies, and horseradish peroxidase (HRP) conjugated secondary anti-rabbit and anti-mouse antibody were purchased from Cell Signaling Technology (Danvers, MA, USA), and β-actin was purchased from Sigma-Aldrich (St. Louis, MO, USA). A Muse® Annexin V and Dead Cell Kit #MCH100105 was purchased from Luminex (Austin, TX, USA). The fluorescent dyes 2′,7′-dichlorodihydrofluorescein diacetate (H_2DCFDA) #2247, and LumiTracker® Mito Green FM #3527 were purchased from Lumiprobe (Moscow, Russia).

3.2. Triterpene Glycosides from the Starfish S. pacificus

3.2.1. Starfish

Specimens of *S. pacificus* Djakonov, 1938 (order Valvatida, family Solasteridae) were collected at a depth of 10–20 m in the Sea of Okhotsk near Iturup Island during the research vessel *Akademik Oparin's* 42nd scientific cruise in August 2012. Species identification was carried out by B.B. Grebnev (G.B. Elyakov Pacific Institute of Bioorganic Chemistry of the FEB RAS, Vladivostok, Russia). A voucher specimen (no. 042-112) is on deposit at the marine specimen collection of the G.B. Elyakov Pacific Institute of Bioorganic Chemistry of the FEB RAS, Vladivostok, Russia.

3.2.2. Isolation of Triterpene Glycosides from the Starfish *S. pacificus*

Cucumarioside D (CucD), pacificusoside D (SpD), pacificusoside F (SpF), pacificusoside H (SpH), and pacificusoside I (SpI) were obtained from the starfish *S. pacificus* by methods published earlier and were pure according to NMR, MS, TLC, and HPLC data [29].

3.3. Bioactivity Assays

3.3.1. Preparation of Triterpene Glycosides

The vehicle control is the cells MDA-MB-231 treated with an equivalent volume of DMSO (final concentration was less than 0.5%) for all presented experiments.

2-Deoxy-D-glucose (2-DG) was dissolved in sterile ddH_2O to prepare stock concentrations of 1 M.

CucD, SpD, SpF, SpH, and SpI from the starfish *S. pacificus* were dissolved in sterile DMSO to prepare stock concentrations of 20 mM.

3.3.2. Cell Lines

Human embryo kidney HEK 293 (ATCC® no. CRL-1573™), and human triple-negative breast cancer cells MDA-MB-231 (ATCC® no. HTB-26™) were purchased from the American Type Culture Collection (Manassas, VA, USA).

3.3.3. Cell Culture Conditions

HEK 293 or MDA-MB-231 cells were maintained in DMEM medium supplemented with 10% fetal bovine serum (FBS), penicillin (100 U/mL), and streptomycin (100 µg/mL). Cultures were incubated in a humidified CO_2-incubator (MCO-18AIC, SANYO, Japan) at 37 °C with 5% CO_2 until cells reached 80–90% confluence. For subculturing, cells were dissociated from flasks using a 0.25% trypsin/0.5 mM EDTA solution. Subsequently, 10–20% of the harvested cells were transferred to new flasks containing fresh complete medium. The number of passages was meticulously controlled, and potential *Mycoplasma* contamination was monitored regularly.

3.3.4. Glucose Uptake, Lactate, and Glutamate Production Assay

MDA-MB-321 cells (2.5×10^4 cells/mL) were seeded in a 96-well plate and cultured at 37 °C in a 5% CO_2 incubator for 24 h. Then the cells were treated with DMSO or 2-DG (0.1, 0.5, and 5 mM) for 24 and 48 h. The culture medium was collected and used to determine the level of lactate production by the Lactate-Glo™ assay kit according to the manufacturer's protocol. The cells attached were washed twice with PBS and used to determine the glucose uptake or level of glutamate production by the Glucose uptake Glo™ assay or Glutamate-Glo™ assay kit, respectively, according to the manufacturer's protocol. The content of glucose and levels of lactate and glutamate were determined by the luminescence method on a PHERAstar FS multi-mode microplate reader (BMG Labtech, Offenburg, Germany) using the appropriate calibration curves.

3.3.5. Cell Viability Assay

MTS Assay

To determine the concentration at which the compounds exert half of their maximal inhibitory effect on cell viability (IC_{50}), HEK 293 or MDA-MB-231 cells (0.8×10^4 cells/200 µL) were treated with either DMSO (vehicle control) or 2-DG at concentrations of 0.1, 0.5, and 5 mM or CucD, SpD, SpF, SpH, and SpI at concentrations of 0.05, 0.1, 0.5, and 1 µM for 24 h. The cells were subsequently incubated with 15 µL of the MTS reagent for 3 h. The absorbance of each well was measured at 490/630 nm on a Power Wave XS microplate reader (BioTek, Winooski, VT, USA).

To determine the effect of 2-DG on cell proliferation, MDA-MB-231 cells were treated with 2-DG (0.1, 0.5, and 5 mM) for 24, 48, and 72 h. The cells were subsequently incubated with 15 µL of the MTS reagent for 3 h. The absorbance of each well was measured at 490/630 nm on a Power Wave XS microplate reader (BioTek, Winooski, VT, USA).

Trypan Blue Exclusion Assay

HEK 293 or MDA-MB-231 cells (0.8×10^4 cells/200 µL) cells were treated with either DMSO (vehicle control) or 2-DG at concentrations of 0.1, 0.5, and 5 mM or CucD, SpD, SpF, SpH, and SpI at concentrations of 0.05, 0.1, 0.5, and 1 µM for 24 h. The culture media was carefully aspirated, and each well was washed with 100 µL of PBS. The cell monolayer was treated with 30 µL of trypsin and incubated for 1 min. The cells were collected with 100 µL PBS and resuspended. Cell suspension was mixed with 0.4% trypan blue (1:1 v/v) and incubated for 1 min at room temperature. The number of live and dead cells was counted using a hemocytometer under a Motic microscope AE 20 (XiangAn, Xiamen, China).

3.3.6. Soft Agar Clonogenic Assay

MDA-MB-231 cells (2.4×10^4 cells/mL) were treated with either DMSO (vehicle control), 2-DG (0.1, 0.5, and 2.5 mM), or triterpene glycosides CucD, SpD, SpF, SpH, or SpI (0.05, 0.1, and 0.2 µM) separately; in the other experiments, the cells were pre-treated with 2-DG (0.5 mM) in combination with SpD (0.025, 0.05, and 0.1 µM). Then the cells were placed onto 0.3% BME agar containing 10% FBS, 2 mM L-glutamine, and 25 µg/mL gentamicin. The cultures were maintained at 37 °C in a 5% CO_2 incubator for 14 days. The number of colonies was counted under an AE 20 Motic microscope using ImageJ software version 1.50i bundled with 64-bit Java 1.6.0_24 (NIH, Bethesda, MD, USA).

3.3.7. Western Blot Assay

MDA-MB-231 cells (1.0×10^5 cells/mL) were seeded in 100 mm dishes and incubated for 24 h at 37 °C in a CO_2 incubator. The cells were pre-treated with either DMSO (vehicle control) or 2-DG (0.5 mM) for 24 h and then treated with SpD at (0.025, 0.05, and 0.1 µM) for an additional 24 h. The preparations of the cell lysate and the Western blot assay. The protein content was determined by the DC protein assay (Bio-Rad, Hercules, CA, USA). Lysates of protein (20–40 µg) were exposed to 10% or 12% SDS-PAGE and electrophoretically transferred to polyvinylidene difluoride membranes (PVDF) (Millipore, Burlington, MA, USA). The membranes were blocked with 5% non-fat milk (Bio-Rad) for 1 h and then incubated with the respective specific primary antibody at 4 °C overnight. Protein bands were visualized using an enhanced chemiluminescence reagent (ECL) (Bio-Rad, Hercules, CA, USA) after hybridization with an HRP-conjugated secondary antibody. The relative expression level was quantified using the Quantity One 1D analysis software, version 4.6.7 (Bio-Rad).

3.3.8. ROS Level Determination Assay

Reactive oxygen species (ROS) determined by staining of MDA-MB-231 cells with fluorescent dye 2′,7′-dichlorodihydrofluorescein diacetate (H_2DCFDA) using previously published method with modifications [61]. In brief, MDA-MB-231 cells (0.5×10^5 cells/mL) were seeded in 60 mm dishes and cultured in DMEM/10% FBS for 24 h at 37 °C in a CO_2-incubator. The attached cells were pre-treated with either DMSO (vehicle control) or 2-DG (0.5 mM) for 24 h, and then treated with SpD at concentrations of 0.025, 0.05, and 0.1 µM for an additional 24 h. Cells were treated with H_2DCFDA (10 µM) and incubated for 30 min at 37 °C. After incubation, cells were washed with PBS, and 5 mL of DMEM/10 FBS was added. The images were taken under CELENA® X High Content Imaging System (Logos Biosystems, Anyang-si, Gyeonggi-do, South Korea) at 10× objective magnification. The intensity of fluorescence microscopic images was determined using cell-integrated CELENA® X Cell Analyzer software version 1.6.0 and the ImageJ software version 1.50i bundled with 64-bit Java 1.6.0_24 (NIH, Bethesda, MD, USA).

For fluorescence spectrometry analysis, MDA-MB-231 cells (2×10^4 cells/200 µL), staining with H_2DCFDA (10 µM), were loaded in black, clear-bottom 96-well plates and fluorescence intensity was measured using a Synergy H1 multimode microplate reader (BioTek, Winooski, VT, USA). Excitation and emission wavelengths were set at 488 nm and 530 nm, respectively, corresponding to the optimal spectral properties of H_2DCFDA. All measurements were performed in triplicate across at least three independent replicates. Background fluorescence (dye-only control without cells) was subtracted from all readings, and data are expressed as mean ± SD relative fluorescence units (RFU).

3.3.9. Mitochondrial Mass Determination Assay

Changes in mitochondrial mass were assessed using MitoTracker Green staining as described earlier [62]. In brief, MDA-MB-231 cells (1×10^5 cells/mL) were seeded in 60 mm dishes and cultured in DMEM/10% FBS for 24 h at 37 °C in a CO_2-incubator. The attached cells were pre-treated with either DMSO (vehicle control) or 2-DG (0.5 mM) for 24 h and then treated with SpD at concentrations of 0.025, 0.05, and 0.1 µM for an additional 24 h. Cells were treated with MitoTracker Green (100 nM) and incubated for 30 min at 37 °C. After incubation, cells were washed with PBS followed by treatment with Hoechst 33342 (1 µg/mL) in PBS for 10 min at 37 °C. After incubation, cells were washed with PBS, and 5 mL of DMEM/10 FBS was added. The images were taken under CELENA® X High Content Imaging System (Logos Biosystems, South Korea) at 10× objective magnification. The intensity of fluorescence microscopic images was determined using cell-integrated CELENA® X Cell Analyzer software version 1.6.0 and the ImageJ software version 1.50i bundled with 64-bit Java 1.6.0_24 (NIH, Bethesda, MD, USA).

Alterations in mitochondrial mass were also assessed by flow cytometry using MitoTracker Green dye. MDA-MB-231 cells (1×10^6 cells/mL) were incubated with 100 nM MitoTracker Green for 30 min at 37 °C in the dark, followed by two washes with warm PBS to remove unbound dye. Cells were then detached using trypsin-EDTA solution, resuspended in 1 mL of PBS, and analyzed immediately on a NovoCyte flow cytometer and NovoExpress flow cytometry software (version 1.6.1) (Agilent Technologies, Santa Clara, CA, USA).

3.3.10. Muse Annexin V and Dead Cell Assay

The apoptosis profile for MDA-MB-231 cells under the treatment by 2-DG was determined using the Muse Annexin V and dead cell kit (Millipore, Billerica, MA, USA) according to the user's guide and the manufacturer's instructions. In brief, MDA-MB-231 cells (1×10^5 cells/mL) were seeded in 60 mm dishes and cultured in DMEM/10% FBS for 24 h at 37 °C in a CO_2-incubator. The attached cells were pre-treated with either DMSO (vehicle control) or 2-DG (0.5 mM) for 24 h and then treated with SpD at concentrations of 0.025, 0.05, and 0.1 µM for an additional 24 h. The cells were washed twice with PBS and harvested with trypsin-EDTA. The TNBC cells MDA-MB-231 (1×10^5 cells/mL) were resuspended in DMEM/10% FBS medium, and 100 µL of cell suspension was added to each tube together with 100 µL of the Muse™ Annexin V and dead cell reagent. The samples were mixed thoroughly by vortexing at a medium speed for 3 to 5 s and were then stained at room temperature in the dark for 20 min, before being analyzed by flow cytometry Muse Cell Analyzer (Millipore, Billerica, MA, USA). The percentage of live, early apoptotic, late apoptotic, and dead cells was estimated using the Muse analysis v.1.8 software.

3.3.11. Statistical Analysis

All the assays were performed in at least triplicate. The results were expressed as mean ± standard deviation (SD). The obtained data were statistically processed by the

one-way analysis of variance (ANOVA) and Tukey's HSD test with significance levels of * $p < 0.05$ and ** $p < 0.01$.

4. Conclusions

Triple-negative breast cancer (TNBC) cells evade metabolic inhibition through adaptive mechanisms shifting from glycolysis to OXPHOS in response to the glycolytic inhibitor 2-DG. This study addresses this challenge by elucidating a novel combination strategy to exploit this vulnerability.

For the first time, the pacificusoside D (SpD) from the starfish *S. pacificus,* in combination with glycolytic inhibitor 2-DG, was demonstrated to effectively inhibit colony formation via targeting the OXPHOS pathway. While low-dose 2-DG induced a pro-survival metabolic shift toward OXPHOS in MDA-MB-231 cells, the co-treatment with SpD at non-cytotoxic concentrations provided a potent synergistic effect, significantly suppressing the formation and growth of colonies in MDA-MB-231 cells. The molecular mechanism underlying the synergistic effect of SpD with 2-DG involves the upregulation of the expression level of the tumor suppressor VHL and subsequent downregulation of the expression level of mitochondrial electron transport chain components. This impairment induces mitochondrial dysfunction, leading to ROS accumulation and the activation of Bax/Bak-mediated intrinsic apoptosis in MDA-MB-231 cells, as confirmed by the upregulation of initiator and effector caspases.

These key findings warrant comprehensive in vivo studies on the bioavailability, efficacy, and safety of starfish-derived triterpene glycosides. Such investigations could refine therapeutic strategies for aggressive breast cancers, ultimately advancing precision oncology.

Author Contributions: O.S.M.: Conceptualization, Methodology (Biological), writing—original draft; T.V.M.: Methodology (Chemical), writing—original draft preparation; A.A.K.: Methodology (Chemical), writing—review and editing; S.P.E.: Funding acquisition, Writing—review and editing; N.V.I.: Supervision, Writing—review and editing. All authors have read and agreed to the published version of the manuscript.

Funding: This research was funded by the Russian Science Foundation (RSF) # 25-14-00100.

Institutional Review Board Statement: Not applicable.

Data Availability Statement: The data presented in this study are available in the article.

Acknowledgments: The study was carried out using the equipment of the Collective Facilities Center "The Far Eastern Center for Structural Molecular Research (NMR/MS)", G.B. Elyakov Pacific Institute of Bioorganic Chemistry, Far Eastern Branch, Russian Academy of Sciences. We are grateful to Anastasia Zueva for her assistance in the experiment determining the metabolic profile of TNBC MDA-MB-231 cells.

Conflicts of Interest: The authors declare no conflict of interest.

References

1. World Health Organization. Breast Cancer. Available online: https://www.who.int/news-room/fact-sheets/detail/breast-cancer (accessed on 14 August 2025).
2. Bray, F.; Laversanne, M.; Sung, H.; Ferlay, J.; Siegel, R.L.; Soerjomataram, I.; Jemal, A. Global cancer statistics 2022: GLOBOCAN estimates of incidence and mortality worldwide for 36 cancers in 185 countries. *CA Cancer J. Clin.* **2024**, *74*, 229–263. [CrossRef]
3. Carvalho, E.; Canberk, S.; Schmitt, F.; Vale, N. Molecular subtypes and mechanisms of breast cancer: Precision medicine approaches for targeted therapies. *Cancers* **2025**, *17*, 1102. [CrossRef] [PubMed]
4. Dai, X.; Li, Y.; Bai, Z.; Tang, X.Q. Molecular portraits revealing the heterogeneity of breast tumor subtypes defined using immunohistochemistry markers. *Sci. Rep.* **2015**, *5*, 14499. [CrossRef] [PubMed]

5. Obidiro, O.; Battogtokh, G.; Akala, E.O. Triple negative breast cancer treatment options and limitations: Future outlook. *Pharmaceutics* **2023**, *15*, 1796. [CrossRef] [PubMed]
6. Zhou, H.L.; Chen, D.D. Prognosis of patients with triple-negative breast cancer: A population-based study from SEER database. *Clin. Breast Cancer* **2023**, *23*, e85–e94. [CrossRef]
7. Akbari, B.; Hasan, M.M.; Islam, S.M. Advances in targeted therapy for triple-negative breast cancer: A review of key antigens and recent advances. *J. Drug Target* **2025**, *33*, 1555–1574. [CrossRef]
8. Pont, M.; Marques, M.; Sorolla, A. Latest therapeutical approaches for triple-negative breast cancer: From preclinical to clinical research. *Int. J. Mol. Sci.* **2024**, *25*, 13518. [CrossRef]
9. Xiong, N.; Wu, H.; Yu, Z. Advancements and challenges in triple-negative breast cancer: A comprehensive review of therapeutic and diagnostic strategies. *Front. Oncol.* **2024**, *14*, 1405491. [CrossRef]
10. Ahuja, S.; Zaheer, S. Molecular mediators of metabolic reprogramming in cancer: Mechanisms, regulatory networks, and therapeutic strategies. *Immunology* **2026**, *177*, 1–43. [CrossRef]
11. Liu, S.; Zhang, X.; Wang, W.; Li, X.; Sun, X.; Zhao, Y.; Wang, Q.; Li, Y.; Hu, F.; Ren, H. Metabolic reprogramming and therapeutic resistance in primary and metastatic breast cancer. *Mol. Cancer* **2024**, *23*, 261. [CrossRef]
12. O'Neill, S.; Porter, R.K.; McNamee, N.; Martinez, V.G.; O'Driscoll, L. 2-Deoxy-D-glucose inhibits aggressive triple-negative breast cancer cells by targeting glycolysis and the cancer stem cell phenotype. *Sci. Rep.* **2019**, *9*, 3788. [CrossRef] [PubMed]
13. Dey, S.; Murmu, N.; Mondal, T.; Saha, I.; Chatterjee, S.; Manna, R.; Haldar, S.; Dash, S.K.; Sarkar, T.R.; Giri, B. Multifaceted entrancing role of glucose and its analogue, 2-deoxy-D-glucose in cancer cell proliferation, inflammation, and virus infection. *Biomed. Pharmacother.* **2022**, *156*, 113801. [CrossRef] [PubMed]
14. Pajak, B.; Siwiak, E.; Soltyka, M.; Priebe, A.; Zielinski, R.; Fokt, I.; Ziemniak, M.; Jaskiewicz, A.; Borowski, R.; Domoradzki, T.; et al. 2-Deoxy-D-glucose and its analogs: From diagnostic to therapeutic agents. *Int. J. Mol. Sci.* **2019**, *21*, 234. [CrossRef] [PubMed]
15. Xi, H.; Barredo, J.C.; Merchan, J.R.; Lampidis, T.J. Endoplasmic reticulum stress induced by 2-deoxyglucose but not glucose starvation activates AMPK through CaMKKβ leading to autophagy. *Biochem. Pharmacol.* **2013**, *85*, 463–477. [CrossRef]
16. Mühlenberg, T.; Grunewald, S.; Treckmann, J.; Podleska, L.; Schuler, M.; Fletcher, J.A.; Bauer, S. Inhibition of KIT-glycosylation by 2-deoxyglucose abrogates KIT-signaling and combination with ABT-263 synergistically induces apoptosis in gastrointestinal stromal tumor. *PLoS ONE* **2015**, *10*, e0120531. [CrossRef]
17. Berthe, A.; Zaffino, M.; Muller, C.; Foulquier, F.; Houdou, M.; Schulz, C.; Bost, F.; De Fay, E.; Mazerbourg, S.; Flament, S. Protein N-glycosylation alteration and glycolysis inhibition both contribute to the antiproliferative action of 2-deoxyglucose in breast cancer cells. *Breast Cancer Res. Treat.* **2018**, *171*, 581–591. [CrossRef]
18. Zhang, D.; Li, J.; Wang, F.; Hu, J.; Wang, S.; Sun, Y. 2-Deoxy-D-glucose targeting of glucose metabolism in cancer cells as a potential therapy. *Cancer Lett.* **2014**, *355*, 176–183. [CrossRef]
19. Repas, J.; Zupin, M.; Vodlan, M.; Veranič, P.; Gole, B.; Potočnik, U.; Pavlin, M. Dual effect of combined metformin and 2-deoxy-D-glucose treatment on mitochondrial biogenesis and PD-L1 expression in triple-negative breast cancer cells. *Cancers* **2022**, *14*, 1343. [CrossRef]
20. Sottnik, J.L.; Lori, J.C.; Rose, B.J.; Thamm, D.H. Glycolysis inhibition by 2-deoxy-D-glucose reverts the metastatic phenotype in vitro and in vivo. *Clin. Exp. Metastasis* **2011**, *28*, 865–875. [CrossRef]
21. Cragg, G.M.; Newman, D.J. Natural products: A continuing source of novel drug leads. *Biochim. Biophys. Acta* **2013**, *1830*, 3670–3695. [CrossRef]
22. Newman, D.J.; Cragg, G.M. Natural products as sources of new drugs over the nearly four decades from 01/1981 to 09/2019. *J. Nat. Prod.* **2020**, *83*, 770–803. [CrossRef] [PubMed]
23. Karthikeyan, A.; Joseph, A.; Nair, B.G. Promising bioactive compounds from the marine environment and their potential effects on various diseases. *J. Genet. Eng. Biotechnol.* **2022**, *20*, 14. [CrossRef] [PubMed]
24. Xia, J.M.; Miao, Z.; Xie, C.L.; Zhang, J.W.; Yang, X.W. Chemical constituents and bioactivities of starfishes: An update. *Chem. Biodivers.* **2020**, *17*, e1900638. [CrossRef] [PubMed]
25. Palagiano, E.; De Marino, S.; Minale, L.; Riccio, R.; Zollo, F.; Iorizzi, M.; Carré, J.B.; Debitus, C.; Lucarain, L.; Provost, J. Ptilomycalin A, crambescidin 800 and related new highly cytotoxic guanidine alkaloids from the starfishes *Fromia monilis* and *Celerina heffernani*. *Tetrahedron* **1995**, *51*, 3675–3682. [CrossRef]
26. Aminin, D.L.; Menchinskaya, E.S.; Pisliagin, E.A.; Silchenko, A.S.; Avilov, S.A.; Kalinin, V.I. Anticancer activity of sea cucumber triterpene glycosides. *Mar. Drugs* **2015**, *13*, 1202–1223. [CrossRef]
27. Aminin, D.L.; Pislyagin, E.A.; Menchinskaya, E.S.; Silchenko, A.S.; Avilov, S.A.; Kalinin, V.I. Immunomodulatory and anti-cancer activity of sea cucumber triterpene glycosides. In *Studies in Natural Products Chemistry (Bioactive Natural Products)*; Atta-ur-Rahman, Ed.; Elsevier Science Publisher: Amsterdam, The Netherlands, 2014; Volume 41, pp. 75–94.
28. Kim, S.K.; Himaya, S.W.A. Chapter 20-Triterpene glycosides from sea cucumbers and their biological activities. *Adv. Food Nutr. Res.* **2012**, *63*, 297–319.

29. Malyarenko, T.V.; Malyarenko, O.S.; Kicha, A.A.; Kalinovsky, A.I.; Dmitrenok, P.S.; Ivanchina, N.V. In vitro anticancer and cancer-preventive activity of new triterpene glycosides from the Far Eastern starfish *Solaster pacificus*. *Mar. Drugs* **2022**, *20*, 216. [CrossRef]
30. Malyarenko, O.S.; Malyarenko, T.V.; Usoltseva, R.V.; Kicha, A.A.; Ivanchina, N.V.; Ermakova, S.P. Combined radiomodifying effect of fucoidan from the brown alga *Saccharina cichorioides* and pacificusoside D from the starfish *Solaster pacificus* in the model of 3D melanoma cells. *Biomolecules* **2023**, *13*, 419. [CrossRef]
31. Malyarenko, T.V.; Kicha, A.A.; Kalinovsky, A.I.; Dmitrenok, P.S.; Malyarenko, O.S.; Kuzmich, A.S.; Stonik, V.A.; Ivanchina, N.V. New Triterpene glycosides from the Far Eastern starfish *Solaster pacificus* and their biological activity. *Biomolecules* **2021**, *11*, 419. [CrossRef]
32. Malyarenko, T.V.; Kicha, A.A.; Kuzmich, A.S.; Malyarenko, O.S.; Kalinovsky, A.I.; Popov, R.S.; Dmitrenok, P.S.; Ivanchina, N.V.; Stonik, V.A. New rare triterpene glycosides from Pacific sun star, *Solaster pacificus*, and their anticancer activity. *Mar. Drugs* **2024**, *22*, 19. [CrossRef]
33. Garg, P.; Singhal, G.; Horne, D.; Salgia, R.; Singhal, S.S. Metabolic reprogramming in breast cancer: Pathways driving progression, drug resistance, and emerging therapeutics. *Biochim. Biophys. Acta Rev. Cancer* **2025**, *1880*, 189396. [CrossRef] [PubMed]
34. Zheng, X.; Ma, H.; Wang, J.; Huang, M.; Fu, D.; Qin, L.; Yin, Q. Energy metabolism pathways in breast cancer progression: The reprogramming, crosstalk, and potential therapeutic targets. *Transl. Oncol.* **2022**, *26*, 101534. [CrossRef] [PubMed]
35. Varghese, E.; Samuel, S.M.; Líšková, A.; Samec, M.; Kubatka, P.; Büsselberg, D. Targeting Glucose Metabolism to Overcome Resistance to Anticancer Chemotherapy in Breast Cancer. *Cancers* **2020**, *12*, 2252. [CrossRef] [PubMed]
36. Tufail, M.; Jiang, C.H.; Li, N. Altered metabolism in cancer: Insights into energy pathways and therapeutic targets. *Mol. Cancer* **2024**, *23*, 203. [CrossRef]
37. You, M.; Xie, Z.; Zhang, N.; Zhang, Y.; Xiao, D.; Liu, S.; Zhuang, W.; Li, L.; Tao, Y. Signaling pathways in cancer metabolism: Mechanisms and therapeutic targets. *Signal Transduct. Target. Ther.* **2023**, *8*, 196. [CrossRef]
38. Dwarakanath, B.; Jain, V. Targeting glucose metabolism with 2-deoxy-D-glucose for improving cancer therapy. *Future Oncol.* **2009**, *5*, 581–585. [CrossRef]
39. Bhat, G.R.; Sethi, I.; Sadida, H.Q.; Rah, B.; Mir, R.; Algehainy, N.; Albalawi, I.A.; Masoodi, T.; Subbaraj, G.K.; Jamal, F.; et al. Cancer cell plasticity: From cellular, molecular, and genetic mechanisms to tumor heterogeneity and drug resistance. *Cancer Metastasis Rev.* **2024**, *43*, 197–228. [CrossRef]
40. Borowicz, S.; Van Scoyk, M.; Avasarala, S.; Karuppusamy Rathinam, M.K.; Tauler, J.; Bikkavilli, R.K.; Winn, R.A. The soft agar colony formation assay. *J. Vis. Exp.* **2014**, *92*, e51998.
41. Horibata, S.; Vo, T.V.; Subramanian, V.; Thompson, P.R.; Coonrod, S.A. Utilization of the soft agar colony formation assay to identify inhibitors of tumorigenicity in breast cancer cells. *J. Vis. Exp.* **2015**, *99*, e52727.
42. Munkacsy, G.; Santarpia, L.; Gyorffy, B. Therapeutic potential of tumor metabolic reprogramming in triple-negative breast cancer. *Int. J. Mol. Sci.* **2023**, *24*, 6945. [CrossRef]
43. Wang, Z.; Jiang, Q.; Dong, C. Metabolic reprogramming in triple-negative breast cancer. *Cancer Biol. Med.* **2020**, *17*, 44–59. [CrossRef] [PubMed]
44. Schiliro, C.; Firestein, B.L. Mechanisms of metabolic reprogramming in cancer cells supporting enhanced growth and proliferation. *Cells* **2021**, *10*, 1056. [CrossRef] [PubMed]
45. Briston, T.; Stephen, J.M.; Thomas, L.W.; Esposito, C.; Chung, Y.L.; Syafruddin, S.E.; Turmaine, M.; Maddalena, L.A.; Greef, B.; Szabadkai, G.; et al. VHL-mediated regulation of CHCHD4 and mitochondrial function. *Front. Oncol.* **2018**, *8*, 388. [CrossRef] [PubMed]
46. Nakhle, J.; Rodriguez, A.M.; Vignais, M.L. Multifaceted roles of mitochondrial components and metabolites in metabolic diseases and cancer. *Int. J. Mol. Sci.* **2020**, *21*, 4405. [CrossRef]
47. Shu, H.; Li, R.; Tang, X.; Zhang, Q. A mitochondrial-related gene signature predicts prognosis and immunotherapy response in hepatocellular carcinoma. *Sci. Rep.* **2025**, *15*, 25435. [CrossRef]
48. Sotgia, F.; Lisanti, M.P. Mitochondrial biomarkers predict tumor progression and poor overall survival in gastric cancers: Companion diagnostics for personalized medicine. *Oncotarget* **2017**, *8*, 67117–67128. [CrossRef]
49. Zhang, G.; Zhong, J.; Lin, L.; Liu, Z. Loss of ATP5A1 enhances proliferation and predicts poor prognosis of colon adenocarcinoma. *Pathol. Res. Pract.* **2022**, *230*, 153679. [CrossRef]
50. Wilson, A.J.; Fadare, O.; Beeghly-Fadiel, A.; Son, D.S.; Liu, Q.; Zhao, S.; Saskowski, J.; Uddin, M.J.; Daniel, C.; Crews, B.; et al. Aberrant over-expression of COX-1 intersects multiple pro-tumorigenic pathways in high-grade serous ovarian cancer. *Oncotarget* **2015**, *6*, 21353–21368. [CrossRef]
51. Du, H.; Xu, T.; Yu, S.; Wu, S.; Zhang, J. Mitochondrial metabolism and cancer therapeutic innovation. *Signal Transduct. Target. Ther.* **2025**, *10*, 245. [CrossRef]

52. Murphy, M.P.; Bayir, H.; Belousov, V.; Chang, C.J.; Davies, K.J.A.; Davies, M.J.; Dick, T.P.; Finkel, T.; Forman, H.J.; Janssen-Heininger, Y.; et al. Guidelines for measuring reactive oxygen species and oxidative damage in cells and in vivo. *Nat. Metab.* **2022**, *4*, 651–662. [CrossRef]
53. Chen, W.; Zhao, H.; Li, Y. Mitochondrial dynamics in health and disease: Mechanisms and potential targets. *Signal Transduct. Target. Ther.* **2023**, *8*, 333. [CrossRef] [PubMed]
54. Valero, T. Mitochondrial biogenesis: Pharmacological approaches. *Curr. Pharm. Des.* **2014**, *20*, 5507–5509. [CrossRef] [PubMed]
55. Li, R.L.; Wang, L.Y.; Duan, H.X.; Zhang, Q.; Guo, X.; Wu, C.; Peng, W. Regulation of mitochondrial dysfunction induced cell apoptosis is a potential therapeutic strategy for herbal medicine to treat neurodegenerative diseases. *Front. Pharmacol.* **2022**, *13*, 937289. [CrossRef] [PubMed]
56. Saddam, M.; Paul, S.K.; Habib, M.A.; Fahim, M.A.; Mimi, A.; Islam, S.; Paul, B.; Helal, M.M.U. Emerging biomarkers and potential therapeutics of the BCL-2 protein family: The apoptotic and anti-apoptotic context. *Egypt J. Med. Hum. Genet.* **2024**, *25*, 12. [CrossRef]
57. Wolf, P.; Schoeniger, A.; Edlich, F. Pro-apoptotic complexes of BAX and BAK on the outer mitochondrial membrane. *Biochim. Biophys. Acta Mol. Cell Res.* **2022**, *1869*, 119317. [CrossRef]
58. Dho, S.H.; Cho, M.; Woo, W.; Jeong, S.; Kim, L.K. Caspases as master regulators of programmed cell death: Apoptosis, pyroptosis and beyond. *Exp. Mol. Med.* **2025**, *57*, 1121–1132. [CrossRef]
59. Green, D.R. The mitochondrial pathway of apoptosis: Part I: MOMP and Beyond. *Cold Spring Harb. Perspect. Biol.* **2022**, *14*, a041038. [CrossRef]
60. Mustafa, M.; Ahmad, R.; Tantry, I.Q.; Ahmad, W.; Siddiqui, S.; Alam, M.; Abbas, K.; Moinuddin; Hassan, M.I.; Habib, S.; et al. Apoptosis: A comprehensive overview of signaling pathways, morphological changes, and physiological significance and therapeutic implications. *Cells* **2024**, *13*, 1838. [CrossRef]
61. Kim, H.; Xue, X.; Kim, H.; Xue, X. Detection of total reactive oxygen species in adherent cells by 2′,7′-dichlorodihydrofluorescein diacetate staining. *J. Vis. Exp.* **2020**, *160*, e60682. [CrossRef]
62. Neikirk, K.; Marshall, A.G.; Kula, B.; Smith, N.; LeBlanc, S.; Hinton, A., Jr. MitoTracker: A useful tool in need of better alternatives. *Eur. J. Cell Biol.* **2023**, *102*, 151371. [CrossRef]

Disclaimer/Publisher's Note: The statements, opinions and data contained in all publications are solely those of the individual author(s) and contributor(s) and not of MDPI and/or the editor(s). MDPI and/or the editor(s) disclaim responsibility for any injury to people or property resulting from any ideas, methods, instructions or products referred to in the content.